

## Structure and Thermodynamics of ssDNA Oligomers near Hydrophobic and Hydrophilic Surfaces

Robert M. Elder and Arthi Jayaraman\*

Department of Chemical and Biological Engineering, University of Colorado at Boulder, CO 80309

\*corresponding author: arthi.jayaraman@colorado.edu

This supporting material contains:

- (1) Water shows expected behaviors near a hydrophilic and hydrophobic surface in the absence of DNA;
- (2) Single-stranded DNA (ssDNA) tetramers assume an upright conformation (perpendicular to the surface) at a specific distance from the surface;
- (3) ssDNA adsorbs to a hydrophobic surface in a 'bases-down' orientation, but there is no preferential orientation of the ssDNA on a hydrophilic surface;
- (4) More favorable energy per ssDNA-surface contact area on OEG than on OMe indicates greater strength of hydrophilic interactions compared to hydrophobic interactions;
- (5) Number of water-water hydrogen bonds per water as a function of surface distance in the absence of DNA;
- (6) Water-DNA hydrogen bonds have a higher duration than water-water hydrogen bonds;
- (7) Cytosine oligomers show similar behavior to adenine oligomers (cf. Figure 7 in main text);
- (8) Additional comparisons of ssDNA dimers and tetramers showing expected and unexpected differences;
- (9) Additional details of surface construction and relaxation;
- (10) Additional details of production simulation protocol;
- (11) Diagram of atoms used to define nucleobase plane;
- (12) Details of calculations used for analysis;
- (13) Discussion of limitations to our approach

(1) Water shows expected behaviors near a hydrophilic and hydrophobic surface in the absence of DNA

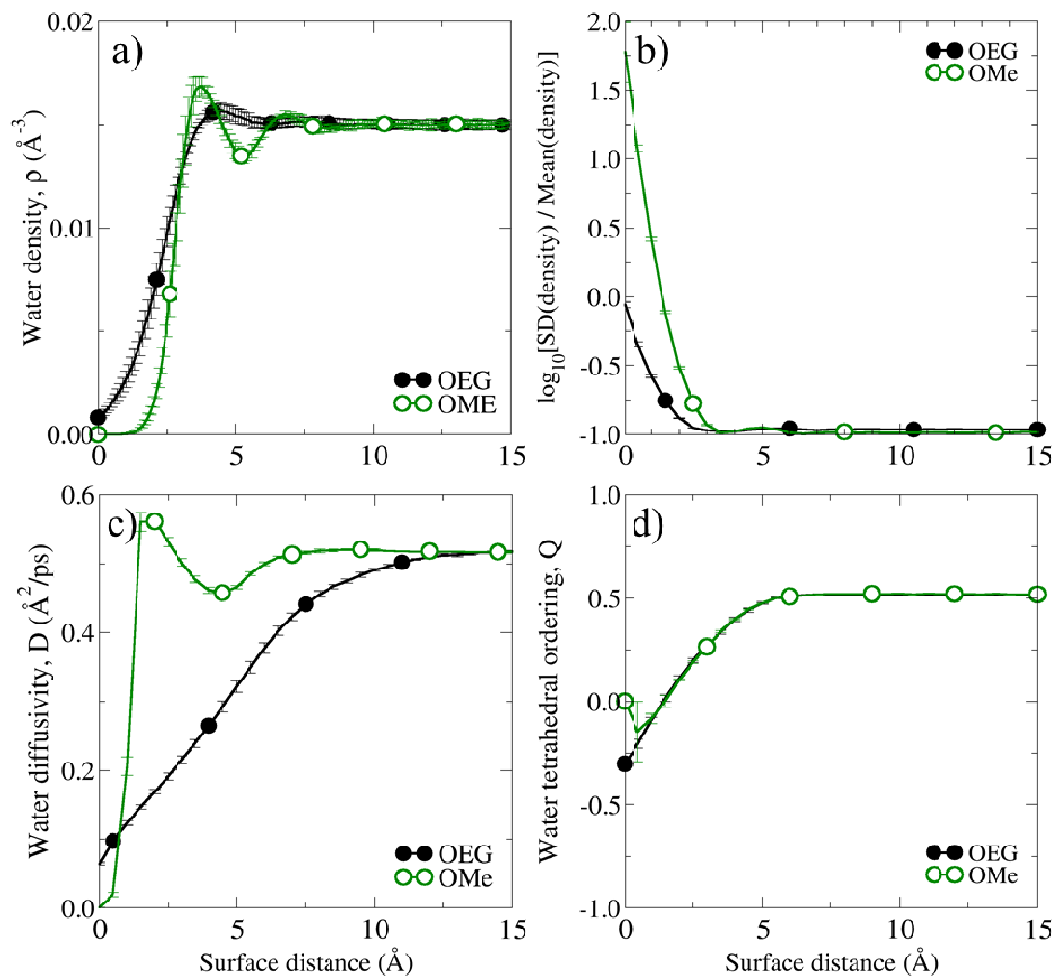


Figure S1. Behavior of water near model hydrophilic (OEG) and hydrophobic (OMe) surfaces. Shown are a) number density,  $\rho$ , b) density fluctuations, c) diffusion coefficient,  $D$ , and d) tetrahedral ordering,  $Q$ , of water as a function of distance from the surface. Density fluctuations are defined as the base-10 logarithm of the standard deviation of the density divided by the mean of the density. With this measure, it is clear that the density fluctuations are much higher near the hydrophobic surface.

Compared to the hydrophilic surface (OEG), water density is lower and density fluctuations are higher near the hydrophobic surface (OMe), as expected (Figure S1a and S1b).<sup>1-3</sup> The effects of the surface on density only extend 5 Å above the surface. Diffusion is slowed substantially from the bulk value near OEG, an effect which extends farther into the bulk water (~10 Å) than the effects on density (Figure S1c). Conversely, water diffusion is unaffected by the hydrophobic surface (OMe) except at shorter ranges, and the effect on diffusion appears to be caused by the changes in water density near the hydrophobic surface: at 3-4 Å, water density increases and diffusion decreases; below 2.5 Å, where the water density is reduced, diffusion increases. These observations are in accord with previous studies of water diffusion near surfaces of varying hydrophobicity.<sup>1, 4</sup> The water self-diffusion coefficient in bulk (~15 Å from the surface) is in quantitative agreement with previous studies of the TIP3P water model in bulk.<sup>5</sup> As expected, the tetrahedral ordering of water is reduced by the presence of a surface (Figure S1d).<sup>6</sup>

(2) Single-stranded DNA (ssDNA) tetramers assume an upright conformation (perpendicular to the surface) at a specific distance from the surface

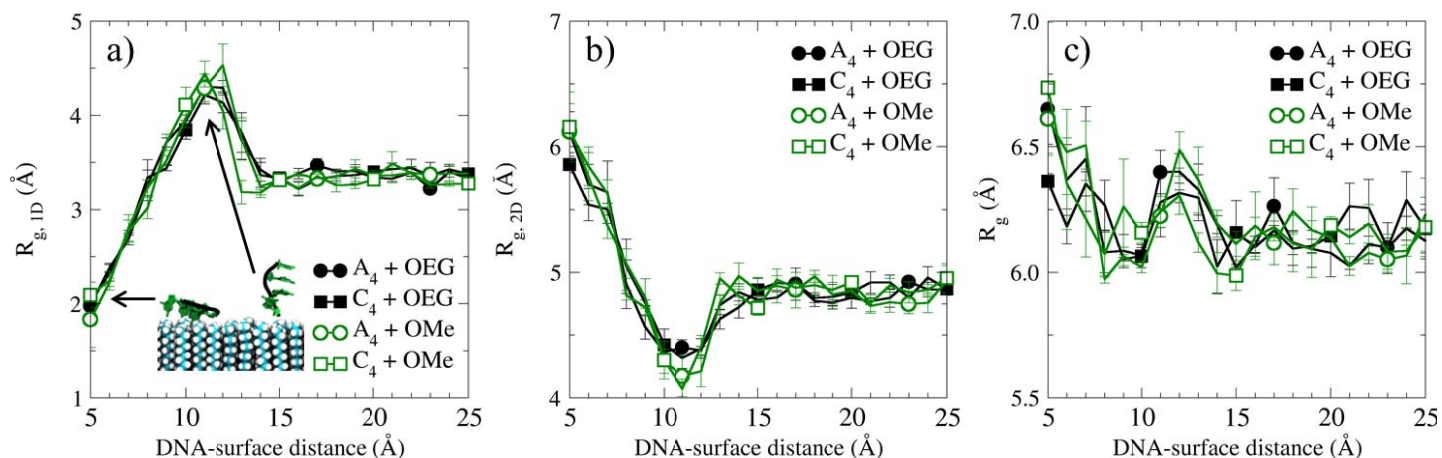


Figure S2. The radius of gyration of the ssDNA in a) the z-direction,  $R_{g,1D}$ , b) the xy-plane,  $R_{g,2D}$ , and c) in all three dimensions,  $R_g$ , as a function of DNA-surface separation distance. Diagram in panel (a) shows parallel and perpendicular (or upright) conformations of ssDNA on the surface at the corresponding values of  $R_{g,1D}$  and DNA-surface distance.

The simultaneous increase of  $R_{g,1D}$  and decrease of  $R_{g,2D}$  between 8-15 Å, relative to the bulk values at distances > 15 Å, indicate that the DNA assumes a conformation perpendicular to the surface. The increase in  $R_{g,2D}$  for distances < 8 Å, and the corresponding decrease in  $R_{g,1D}$ , indicate that the DNA must orient itself parallel to the surface as it approaches very closely, probably due to steric constraints imposed by the surface. The overall  $R_g$  does not change significantly until distances < 8 Å are reached, below which the value of  $R_g$  increases by roughly 10%, probably due to steric constraints imposed by the surface.

(3) ssDNA adsorbs to a hydrophobic surface in a ‘bases-down’ orientation, but there is no preferential orientation of the ssDNA on a hydrophilic surface

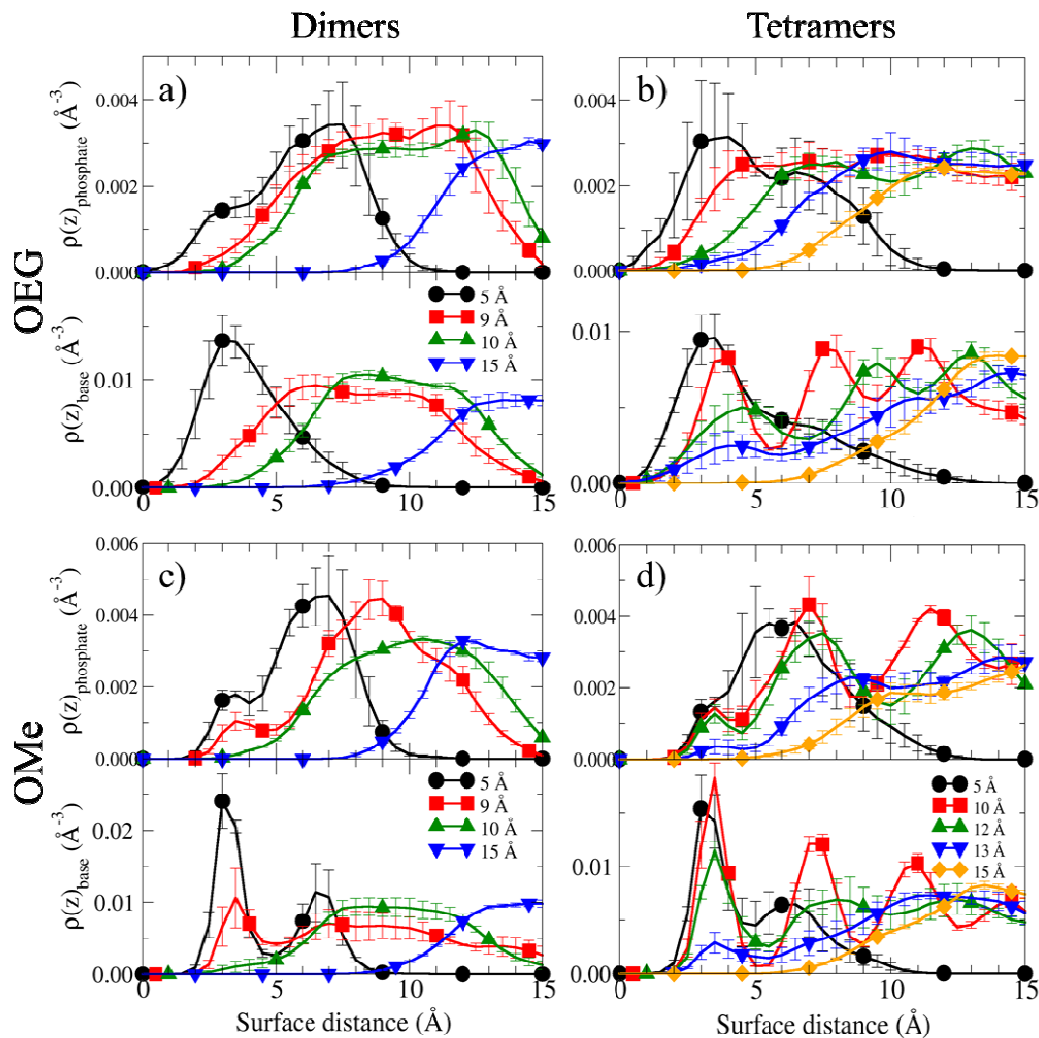


Figure S3. Density distributions of phosphate atoms (top half of each panel) and nucleobase atoms (bottom half of each panel) for **adenine**-based dimers and tetramers when the ssDNA is held at various distances from the indicated surfaces. The legends indicate the distance at which the ssDNA is held from the surface. Phosphate atoms include the phosphorous atom and the four oxygen atoms bonded to the phosphorous atom. Nucleobase atoms include only the atoms that comprise the nucleobases and exclude all sugar and phosphate backbone atoms.

Examining the density distributions on OEG when the ssDNA is held at 5 Å from the surface (black lines in panels (a) and (b)), neither the bases nor the phosphates show a preference for the surface or the bulk; i.e., the base and phosphate density distributions occupy roughly the same spatial region. The same is true on OEG at larger DNA-surface separation distances (e.g., the red lines in panels (a) and (b), where the ssDNA is held at 10 Å from the surface). We interpret this to mean that there is no preferred orientation for adsorption to OEG.

Examining the distributions on OMe, however, shows that the bases preferentially locate at the surface and the phosphates remain farther from the surface. For both ssDNA lengths held at 5 Å from the OMe surface (black lines in panels (c) and (d)), there is a sharp peak in the base density around 3 Å, while the peak in the phosphate density is farther from the surface at 6 Å. For the tetramers on OMe, this pattern persists even at larger DNA-surface separation distances: there is a peak in the base density at 3 Å, and the phosphate density is primarily located at farther distances, at DNA-surface separation distances of 10, 12, and 13 Å. We interpret this to mean that the ssDNA adsorbs preferentially in a ‘bases-

down” conformation where the bases are close to the surface and the phosphates are farther from the surface. This conformation might leave the nucleobases unavailable for base-pairing with other ssDNA strands in bulk solution.

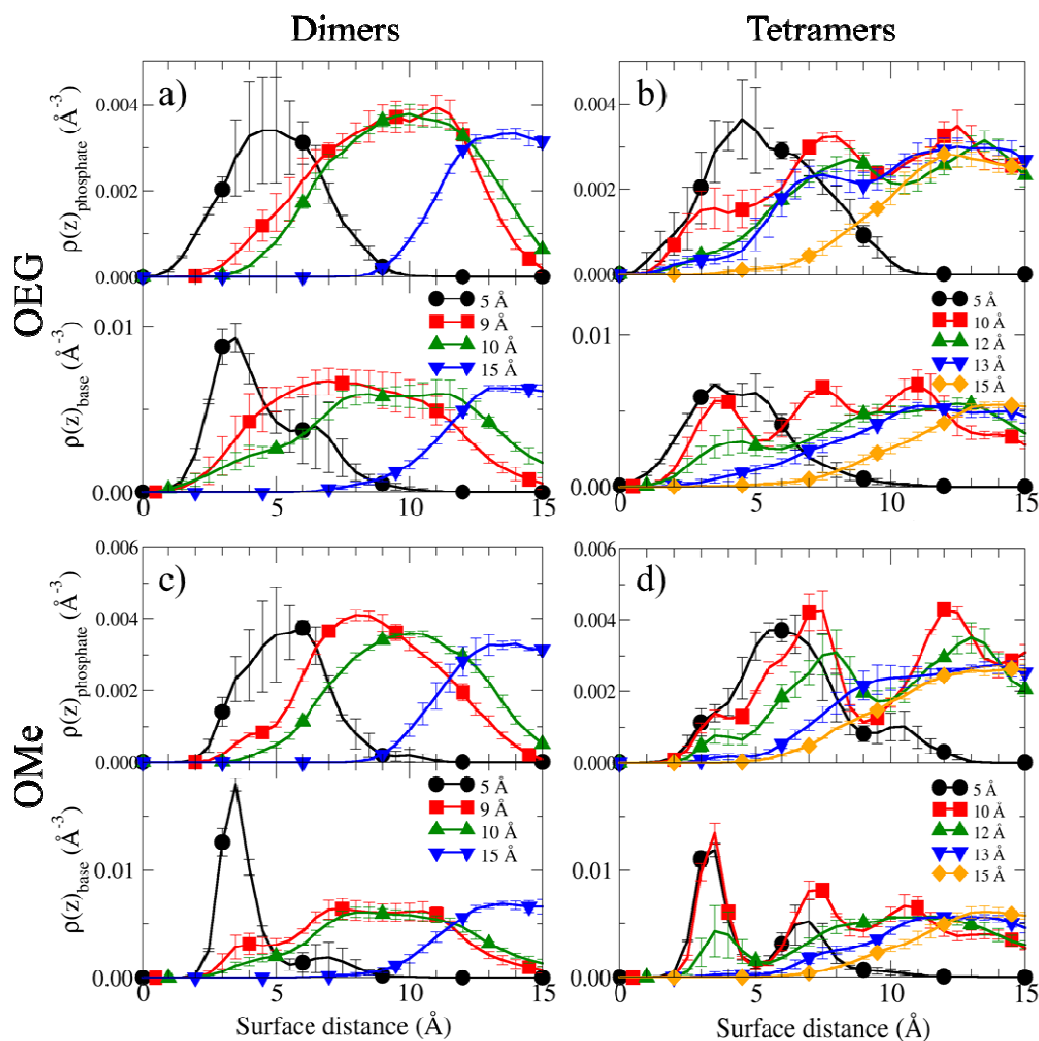


Figure S4. Density distributions of phosphate atoms (top half of each panel) and nucleobase atoms (bottom half of each panel) for **cytosine**-based dimers and tetramers when the ssDNA is held at various distances from the indicated surfaces. The legends indicate the distance at which the ssDNA is held from the surface. Phosphate atoms include the phosphorous atom and the four oxygen atoms bonded to the phosphorous atom. Nucleobase atoms include only the atoms that comprise the nucleobases and exclude all sugar and phosphate backbone atoms.

The same commentary as for Figure S3 applies here: on OMe, the bases locate preferentially to the surface (“base-down”) and the phosphates are farther from the surface; while on OEG, there is no preferred orientation of the bases or phosphates.

- (4) More favorable energy per ssDNA-surface contact area on OEG than on OMe indicates greater strength of hydrophilic interactions compared to hydrophobic interactions

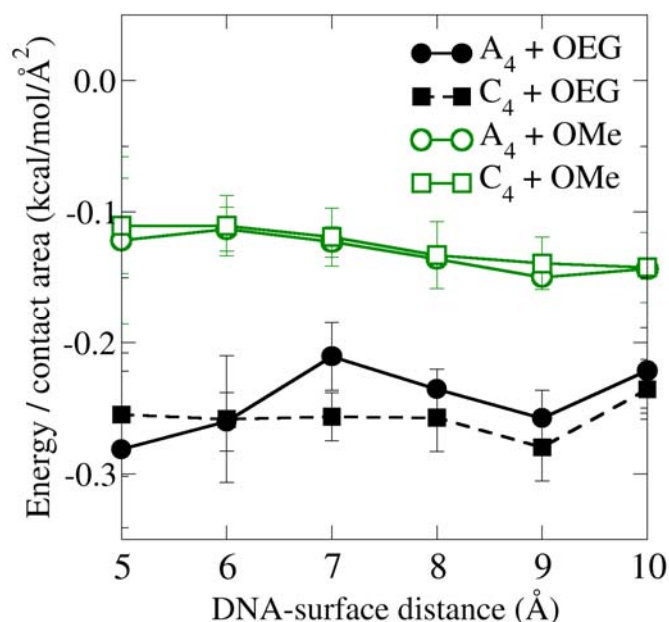


Figure S5. Total non-bonded energy (van der Waals and electrostatic) between ssDNA and the surface divided by the contact area between ssDNA and the surface. Only DNA-surface distances less than 10 Å are shown to omit regions with very low DNA-surface contact area, which lead to physically unreasonable values of this quantity (i.e., long-range interactions do not require direct contact, leading to non-finite values when the contact area is zero). Energy values are negative because the energy between the ssDNA and the surfaces is favorable. The average value on OMe is approximately  $-0.125$  kcal/mol/Å<sup>2</sup>, while the average value on OEG is approximately  $-0.25$  kcal/mol/Å<sup>2</sup>, showing that the energy per contact area on OEG is approximately double that on OMe. We interpret the greater energy per contact area with OEG as evidence that hydrophilic interactions have a stronger enthalpic component than hydrophobic interactions for these systems.

(5) Number of water-water hydrogen bonds per water as a function of surface distance in the absence of DNA

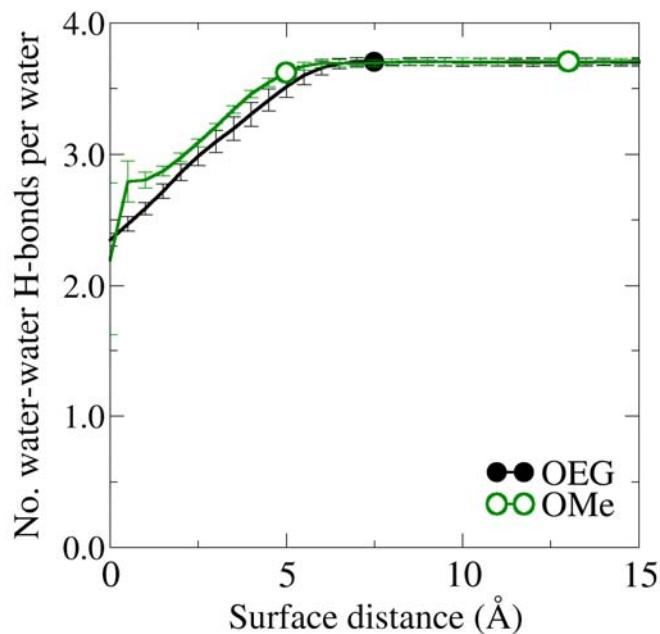


Figure S6. Number of water-water hydrogen bonds per water molecule in the absence of ssDNA as a function of surface distance. The average bulk value (surface distances  $> 5 \text{ \AA}$ ) with our geometric criteria is approximately 3.7 water-water hydrogen bonds per water molecule. Compare this to Figure 6 in the main text, which shows the number of water hydrogen bonds with various molecules, reveals that the water near OEG is more bulk-like than the water near OMe: in the absence of DNA, water molecules near OEG have 3.3 total hydrogen bonds per water molecule, while water molecules near OMe have only 3.1 total hydrogen bonds per water molecule.

(6) Water-DNA hydrogen bonds have a higher duration than water-water hydrogen bonds

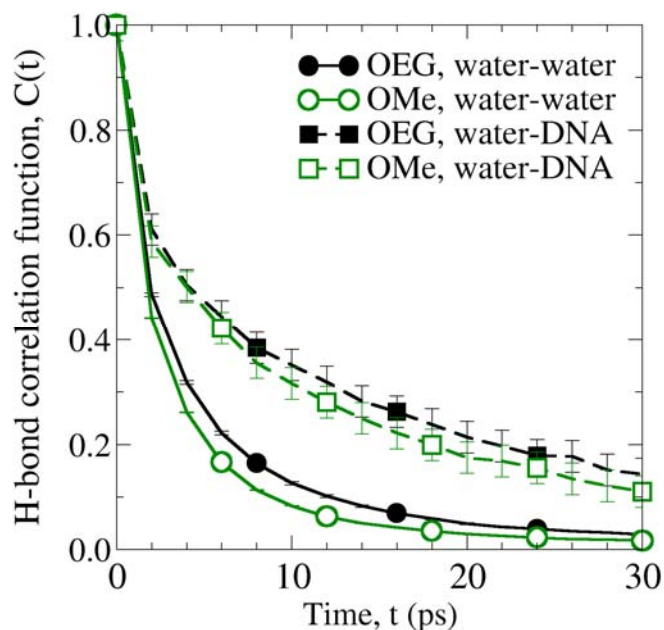


Figure S7. Hydrogen bond time correlation function,  $C(t)$ , of water-water and water-DNA hydrogen bonds. The time correlation function shows the probability that a hydrogen bond still exists at time  $t$  given that it existed at time 0.<sup>7</sup> In calculating the correlation function, we have allowed for hydrogen bonds to break and subsequently reform rather than requiring that they remain continuously intact. This manner of calculation emphasizes the fact that water-DNA hydrogen bonds tend to last for longer periods of time, and re-form after temporarily breaking, by showing a long-lasting tail in the correlation function.<sup>8</sup> Since our interest lies here in the behavior of water molecules near the surface, we only consider water molecules within 5 Å of the topmost heavy atoms of the surfaces. Here, we use simulations of an adenine dimer at a DNA-surface separation distances of 5 Å to calculate the water-DNA hydrogen bond correlation functions; results for cytosine and for tetramers are similar.

Clearly, water-water hydrogen bonds last for a shorter period of time than water-DNA hydrogen bonds. Over 50% of water-water hydrogen bonds break within 2 ps, and only 10% remain after 10 ps. By contrast, approximately two-thirds of the water-DNA hydrogen bonds still exist after 2 ps, and more than 10% remain even after 30 ps.

(7) Cytosine oligomers show similar behavior to adenine oligomers (cf. Figure 7 in main text)

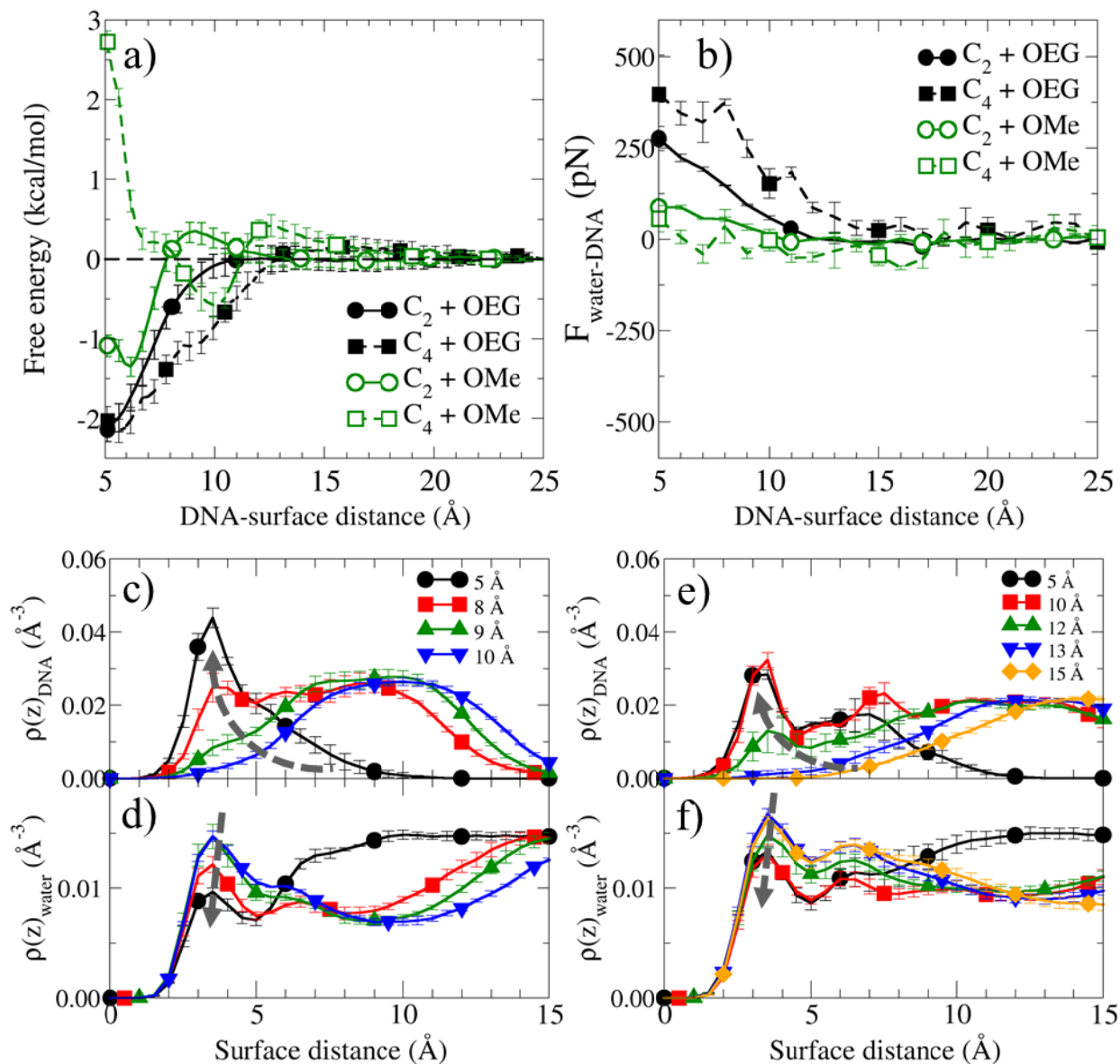


Figure S8. Comparison of (a) free energy of adsorption and (b) force of water on ssDNA for the *cytosine* dimer (circles) or tetramer (squares) adsorbing to OEG or OMe. The density profiles of water (c, e) and DNA (d, f) when the adenine dimer (c, d) or tetramer (e, f) is held at various distances from the OMe SAM. The dashed gray arrows in (c, e) indicate the increasing density of DNA at the surface as the DNA approaches the surface, and the dashed arrows in (d, f) indicate the decreasing water density as the DNA approaches. This figure is intended to demonstrate that the behaviors shown in Figure 7 in the main text, which pertains to *adenine*-based ssDNA, are not limited to adenine bases. See main manuscript for a discussion of the behaviors observed for adenine bases, which also apply to cytosine.

(8) Additional comparisons of ssDNA dimers and tetramers showing expected and unexpected differences

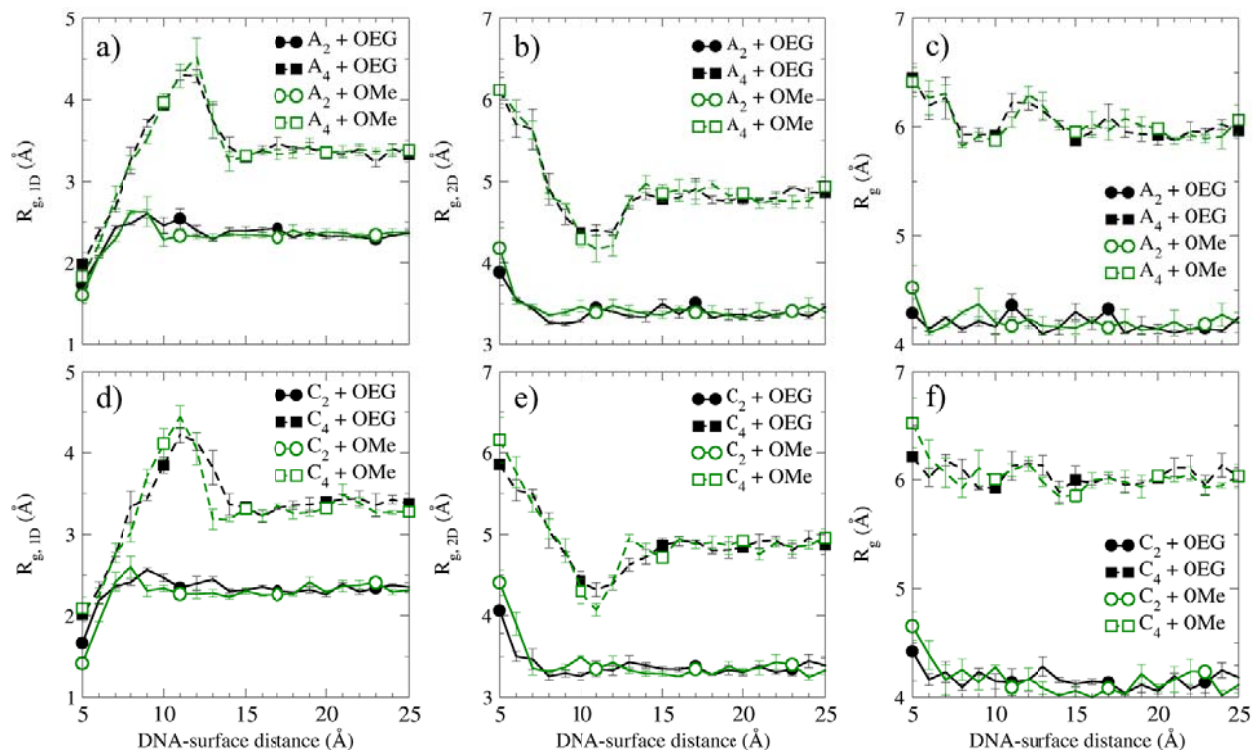


Figure S9. The radius of gyration of the ssDNA in (a, d) the z-direction,  $R_{g,1D}$ , (b, e) the xy-plane,  $R_{g,2D}$ , and (c, f) in all three dimensions,  $R_g$ , as a function of DNA-surface separation distance for (a, b, c) adenine and (d, e, f) cytosine oligomers.

While the tetramers ( $A_4$ ,  $C_4$ ) show significant changes in these three measures of size as the DNA-surface distance decreases below 15 Å (discussed in Figure S2 and the main text), the ssDNA dimers ( $A_2$ ,  $C_2$ ) only show changes in size at very small surface separation distances ( $< 6$  Å). The changes in ssDNA dimer size are most likely due to steric constraints imposed by the surface.

Both the dimers and tetramers reach approximately the same value of  $R_{g,1D}$  at a DNA-surface distance of 5 Å, while the value of  $R_{g,2D}$  for tetramers is nearly double that of dimers at a distance of 5 Å. These observations suggest that both lengths of oligomer lie parallel to the surface at a DNA-surface distance of 5 Å. In a parallel conformation, the long axis of each oligomer (roughly oriented along the DNA backbone) should be parallel to the surface, and consequently the shorter axes of the oligomers should be oriented perpendicular to the surface. The “width” or “depth” of the oligomers (i.e., the shorter axes) should be the same for dimers and tetramers (i.e., approximately the “width” or “depth” of a nucleobase), while the “length” of the oligomers (i.e., the long axis) should be different (i.e., approximately the length of the oligomer backbone). Having  $R_{g,1D}$  similar between the two oligomer lengths and  $R_{g,2D}$  approximately double for the tetramers is therefore consistent with a parallel orientation for both ssDNA lengths at very close surface separation distances.

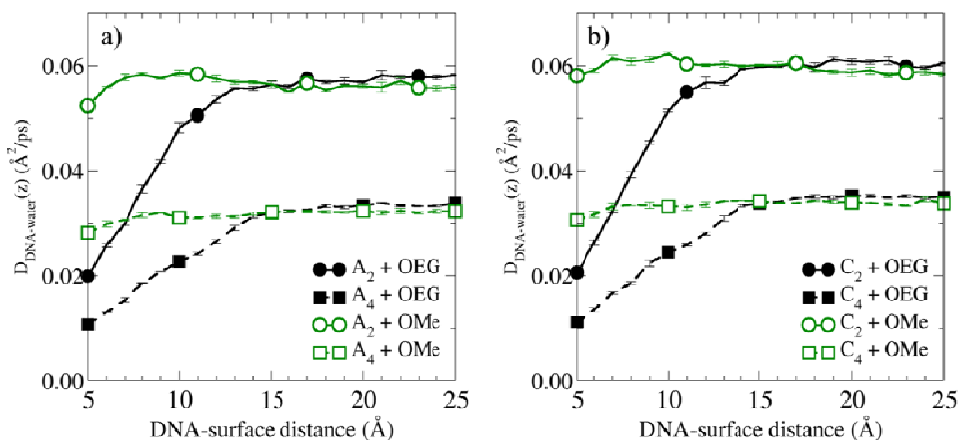


Figure S10. Diffusion coefficients of ssDNA dimers and tetramers of a) adenine and b) cytosine as a function of DNA-surface distance. The behavior of dimers and tetramers is similar, but the diffusion coefficients of tetramers are approximately half that of dimers because the ssDNA tetramers have approximately double the mass of dimers.

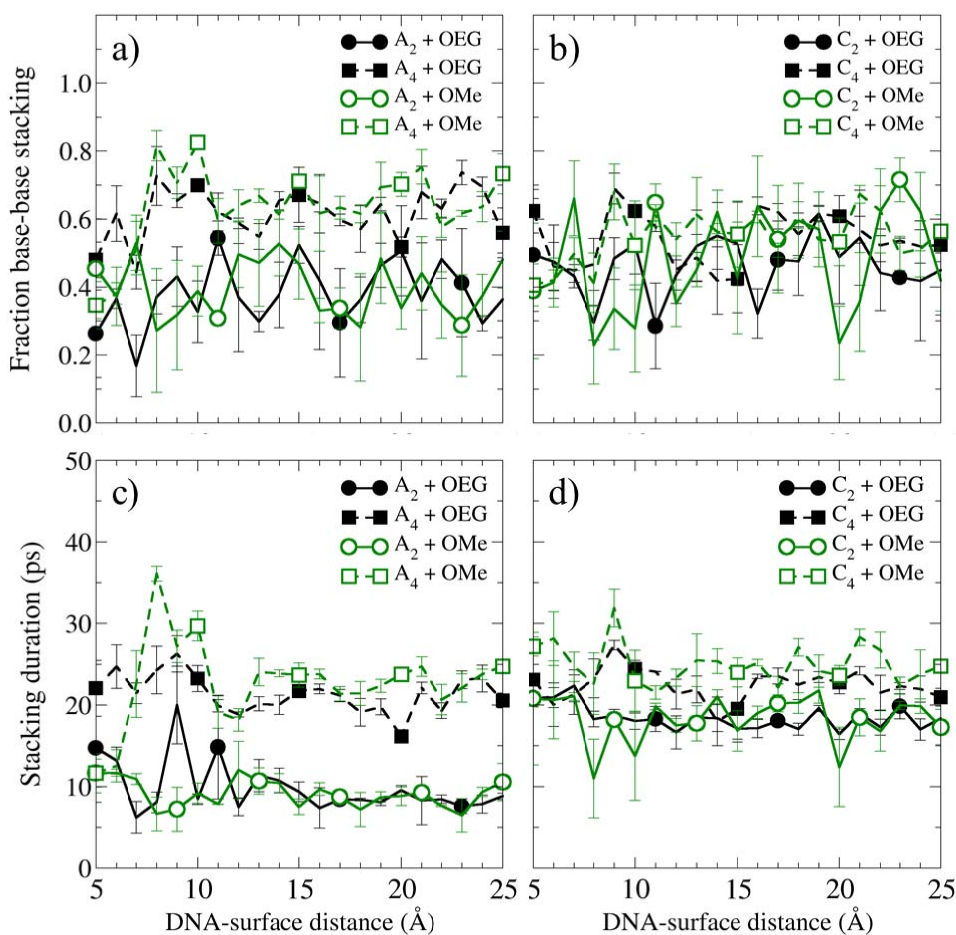


Figure S11. Frequency (a, b) and duration (c, d) of base-base stacking of adenine (a, c) and cytosine (b, d) dimers and tetramers as a function of DNA-surface distance. Please note that the frequency of stacking is normalized to the number of base-base stacking interactions that are possible. Tetramers exhibit both greater frequency and duration of base-base stacking than dimers, corroborating our supposition that increased base-base stacking protects tetramer ssDNA from the

repulsive force of the low-density region of water, while ssDNA dimers experience the full effect of this repulsive force because they are less capable of base-base stacking (see Figure 7 in the main text).

#### (9) Details of surface construction and relaxation

After constructing the surfaces and minimizing their energies to eliminate unfavorable atomic contacts, we use the following protocol to further relax the surfaces into their preferred arrangement. The coordinates of the energy minimized surfaces were solvated with TIP3P water molecules to create a 20 Å thick layer on both the +z and -z sides of the surface. It is convenient to place water molecules on both sides of the surface when using the LEaP program of the Amber suite, and the periodic boundary condition in the z-direction ensures that this is equivalent to having water molecules on only one side (top or bottom) of the surface. Then, to further relax the surfaces, we conducted a series of MD simulations. The initial size of the periodic box for these simulations was carefully chosen to ensure that the periodic images of the surfaces were in close contact, thereby eliminating any gaps in the surfaces and creating an infinite surface when combined with periodic boundary conditions in the x- and y-directions, yielding a cross-sectional area of approximately 6.5 nm by 7 nm. During these simulations, the bottommost heavy atom of each oligomer was constrained to a constant z-value to prevent dissolution of the monolayer while still allowing lateral diffusion and rearrangement in the xy-plane. This constraint on the oligomers was applied with the *collective variables* module of NAMD and a force constant of 2.5 kcal/mol-Å was used. First, we conducted constant temperature (300 K), volume, and number of particles (NVT) MD for 100 ps to allow the water molecules to equilibrate. Next, we conducted constant temperature, constant pressure (1 atm), and constant number of particles (NPT) MD for 100 ps with constant xy-area to allow the pressure to equilibrate while maintaining constant grafting density. Finally, we used the coordinates of these relaxed surfaces – with a predetermined grafting density and now equilibrated in the presence of liquid water – for the remainder of our simulations.

(10) Details of production simulation protocol

After constructing fully-solvated systems including ssDNA, neutralizing Na<sup>+</sup> counterions, the self-assembled monolayer (SAM), we used the following procedure to carefully equilibrate the systems prior to use in umbrella sampling simulations. First, in constant volume and temperature conditions (NVT ensemble), the water and ions were minimized with the conjugate gradient algorithm for 2000 steps, with the DNA and SAM subjected to a 500 kcal/mol-Å<sup>2</sup> harmonic restraining potential. Second, in the NVT ensemble, with the DNA/SAM restraining potential reduced to 100 kcal/mol-Å<sup>2</sup>, the system was heated from 0 to 300 K over 20 ps. Third, in constant pressure and temperature conditions (NPT ensemble) and with the restraint reduced to 50 kcal/mol-Å<sup>2</sup> the system was relaxed for another 20 ps. Fourth, in the NVT ensemble, the restraining potential was reduced in three steps (50, 10, and 5 kcal/mol-Å<sup>2</sup>) and minimized for 2000 steps each. Fifth, in the NVT ensemble with the same 5 kcal/mol-Å<sup>2</sup> restraint the system was heated from 10 to 300 K over 20 ps. Sixth, in the NPT ensemble, the restraint was reduced from 5 to 1 to 0.1 to 0 kcal/mol-Å<sup>2</sup> over 20 ps. Seventh, in the NVT ensemble with no restraints, the system was heated from 10 to 300 K over 20 ps. Finally, the system was heated from 100 to 300 K over 20 ps in the NPT ensemble at the beginning of each production run. A Langevin thermostat and barostat were used to control the temperature (damping coefficient of 1 ps<sup>-1</sup>) and pressure (piston period of 100 fs and piston decay constant of 50 fs) at 300 K and 1 atm. The SHAKE<sup>9</sup> algorithm was used to constrain all bonds involving hydrogen, and a time step of 2 fs was used. Electrostatic interactions were treated with the particle-mesh Ewald (PME) summation method<sup>9</sup>, with a tolerance of 1e-6 and interpolation order of 4. The non-bonded cutoff was 9.0 Å and the non-bonded list was updated every 10 steps. Snapshots were recorded every 2 ps.

(11) Diagram of atoms used to define nucleobase plane

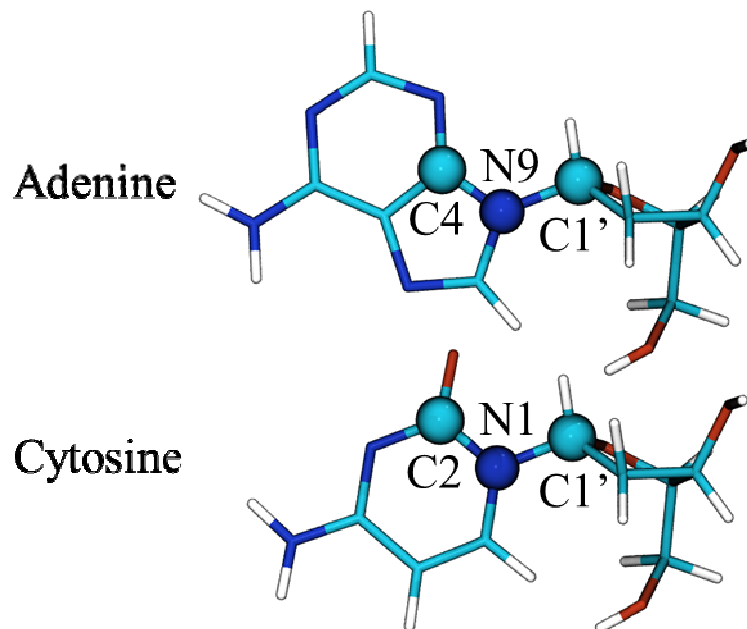


Figure S12. Diagram of atoms (shown as spheres) used to define the nucleobase plane of adenine and cytosine. The direction of the base plane normal is given by the cross product  $(N1-C1') \times (N1-C2)$  for cytosine and  $(N9-C1') \times (N9-C4)$  for adenine, where  $(X-Y)$  is the vector pointing from atom Y to atom X.<sup>10</sup>

## (12) Details of calculations used for analysis

We assess hydrogen bonding with a geometric criterion involving the three atoms that participate in the hydrogen bond (donor, acceptor, and hydrogen): if the distance between the donor and acceptor is less than 3.5 Å and the angle formed by the three atoms is greater than 120° (i.e., the angle is within 60° of 180°), they are characterized as forming a hydrogen bond (see Figure 3b for diagram). We quantify the hydrogen bonding duration and frequency, the latter of which is defined as the percentage of simulation time that a particular type of hydrogen bond is formed. When we calculate hydrogen bonds between the DNA and other molecules, we consider all possible hydrogen bonding partners (donors and acceptors) on the ssDNA rather than only the Watson-Crick hydrogen bonding partners. We also normalize the frequency to the total number of hydrogen bonding partners on the ssDNA to allow comparisons between different DNA bases with different total numbers of hydrogen bonding partners.

Base-base stacking is quantified by applying a geometric criterion involving the distance between two bases and the normal vectors of the planes of the two bases involved. In keeping with standard practice,<sup>10</sup> we define the base plane by the plane formed between three atoms in each nucleobase: N9, C4, and C1' for purines and N1, C2, and C1' for pyrimidines (see Supporting Figure S12 for diagram). If the angle between the normal of two base planes is less than 45° and the distance between the centers of mass of the two nucleobases is less than 4.5 Å, we consider the bases stacked. These geometric cut-offs are chosen because they yield approximately 90% stacking in B-form double-stranded DNA. We introduce another form of analysis, related to base-base stacking, to quantify hydrophobic interactions between the DNA and the surface. These “face-on” conformations, where a DNA base is lying parallel against the surface, facilitate hydrophobic interactions between the DNA and the surface. If the center of mass of a base is within 4.5 Å in the z-direction of the center of mass of the topmost heavy atoms in the surface and the base normal is within 45° of the surface normal, which we define as the z-axis for simplicity, we consider the base to be interacting “face-on” with the surface (see Figure 3d for diagram). The base normal for a face-on conformation is defined in the same way as for base-base stacking. As with hydrogen bonds, we quantify the duration and frequency of base-base stacking and face-on conformations, and we normalize the frequency (i.e., the percentage of the entire simulation time that an interaction occurs) to the total possible number of base-base stacking interactions or face-on conformations.

We calculate the radius of gyration ( $R_g$ ) of the ssDNA as:  $R_g = \sqrt{\frac{1}{N} \sum_{k=1}^N (r_k - r_{COM})^2}$ , where  $N$  is the number of atoms comprising the ssDNA,  $r_k$  is the coordinates of atom  $k$ , and  $r_{COM}$  is the center-of-mass of the ssDNA. We choose  $r_k$  and  $r_{COM}$  to be three-dimensional (x-, y-, and z-coordinates) for the standard measure of  $R_g$ , two-dimensional (x- and y-coordinates) to calculate the radius of gyration in the xy-plane ( $R_{g,2D}$ ), or one-dimensional (z-coordinate only) to calculate the radius of gyration in the z-direction ( $R_{g,1D}$ ).

For some calculations, we wish to limit the analysis to only those water molecules that are between the DNA and the surface. To accomplish this, we only use water molecules that are within a cylindrical region of space between the DNA and the surface (see Figure 5a for a diagram). The radius of the cylinder is given by the two-dimensional radius of gyration in the xy-plane ( $R_{g,2D}$ ) of the ssDNA, and the cylinder extends vertically (perpendicular to the surface in the z-direction) from the center of mass of the topmost heavy atoms of the surface upward to the center of mass of the DNA.

We calculate the axial density distribution function,  $\rho(z)$ , of all water and ssDNA atoms as a function of distance from the surface in the +z-direction:  $\rho(z) = N(z)/V_{slab}$ , where  $N(z)$  is the number of atoms within 0.5 Å of the z-value within, and  $V_{slab}$  is the volume of the rectangular slab at each z-distance (0.5 Å slab height multiplied by the cross-sectional area of the simulation box). For some calculations, we calculate the density distribution function in the same cylindrical region defined in the previous paragraph; for these calculations, we use cylindrical slices of the cylindrical region instead of rectangular slabs of the entire simulation box. We report the density as the number density of the atoms of interest (i.e., water or DNA atoms).

The diffusivity,  $D$ , of a molecule is calculated using a finite-difference approximation:  $D = (|r(t_2) - r(t_0)|^2 - |r(t_1) - r(t_0)|^2) / (2d(t_2 - t_1))$ , where  $r$  is the coordinate vector of the molecule in question, which may be 1-, 2-, or 3-dimensional,  $t$  is the time, for which the subscripts (0, 1, 2) indicate three consecutive simulation snapshots, and  $d$  is the dimensionality of  $r$  (1, 2, or 3).<sup>1</sup> Angular brackets denote averaging over all times. Note that the quantity  $(t_2 - t_1)$  is the

length of a single simulation snapshot. To calculate the diffusivity of ssDNA, we use the center of mass of the DNA as the coordinate  $r$ , while for water molecules we use the coordinate of the oxygen atom. To ensure that the lateral diffusion of the DNA was not affected by the umbrella sampling bias (i.e., no coupling of diffusion in the z-direction to diffusion in the x- and/or y-directions, or, equivalently, a diagonal diffusion tensor) we calculated the off-diagonal components of the diffusion tensor ( $D_{xy}$ ,  $D_{xz}$ ,  $D_{yz}$ ). We used the formalism shown in eq. 6 of Raspopovic *et al.*<sup>11</sup> In this formalism, the off-diagonal components are calculated as  $D_{ij} = \frac{1}{2} \frac{d(\langle ij \rangle - \langle i \rangle \langle j \rangle)}{dt} = \frac{1}{2} (\langle i v_j \rangle + \langle j v_i \rangle - \langle i \rangle \langle v_j \rangle - \langle j \rangle \langle v_i \rangle)$ , where  $i$  and  $j$  are the x, y, and z coordinates,  $v_i$  is the velocity in the  $i$  direction, and angular brackets indicate ensemble averaging. This calculation assumes that the diffusion tensor is symmetric. We estimated the velocity at each time step  $t$  using a central difference approximation with time steps  $t+1$  and  $t-1$ . We found that all three off-diagonal components are essentially zero (data not shown), indicating that there is no coupling between the umbrella sampling bias and lateral diffusion.

We also calculate the tetrahedral ordering of water. The tetrahedral ordering parameter of water oxygen atom  $k$ ,  $Q_k$ , is defined by:  $Q_k = 1 - \frac{3}{8} \sum_i^3 \sum_{j=i+1}^4 \left[ \cos \phi_{ikj} + \frac{1}{3} \right]^2$ , where  $i$  and  $j$  iterate over the 4 nearest water oxygen atoms to water oxygen atom  $k$ , and  $\phi_{ikj}$  is the angle between atoms  $i$ ,  $k$ , and  $j$ .<sup>12</sup> For this calculation to function properly, the two vectors defining  $\phi_{ikj}$  must point from the central atom  $k$  to the atoms  $i$  and  $j$  (i.e.,  $r_{ik} = r_i - r_k$ , where  $r_k$  is the Cartesian coordinate of the atom  $k$ ). A value of  $Q_k = 1$  indicates perfect tetrahedral ordering, a value of  $Q_k = 0$  indicates random ordering (e.g. an ideal gas), and values of  $Q_k < 0$  are possible. We average the value of  $Q_k$  over all water oxygen atoms of interest and over all simulation times, and we denote this average value simply as  $Q$ . Note that we do not include non-water atoms (e.g., atoms in the surface) in the calculation of  $Q$  as is sometimes done.<sup>6</sup>

The non-bonded forces and energies between the ssDNA and other components of the system are calculated using the pair interaction feature of NAMD.<sup>13</sup> We only report the forces in the z-direction because the x- and y-components average to zero.

(13) Discussion of limitations to our approach

We have touched on the limitations to our approach in the main text, but we explicitly state and discuss some of these limitations here. First, there are the limitations inherent in any simulation approach, such as the approximate nature of the force field defining the intra- and intermolecular interactions, including the estimation of atomic partial charges. However, our primary interest is in creating idealized hydrophilic and hydrophobic surfaces rather than studying self-assembled monolayers with specific chemistries, and we have shown that our idealized surfaces produce the intended environments by verifying that they produce the expected behaviors of water in hydrophilic and hydrophobic environments. Second, care must be taken in making comparisons between our idealized surfaces and experimentally studied self-assembled monolayers (SAMs). For instance, most OEG SAMs have somewhat lower coverage than the surface we have constructed, and the most effective surface coverage for preventing protein adsorption has been shown to be approximately  $2/3$ .<sup>4</sup> Therefore, real surfaces with lower coverage may exhibit weaker ssDNA adsorption than we have found. Similarly, surfaces with different chemistry, such as a methoxy-terminated OEG instead of our hydroxyl-terminated OEG, will likely have different properties.<sup>14</sup> Bearing these limitations in mind, we have found interesting behaviors that could be used to understand more complicated systems and to optimize the adsorption of ssDNA.

### Supporting References

1. J. Feng, K.-Y. Wong, K. Dyer and B. M. Pettitt, *J. Chem. Phys.*, 2009, **131**, 125102-125108.
2. A. Poynor, L. Hong, I. K. Robinson, S. Granick, Z. Zhang and P. A. Fenter, *Phys. Rev. Lett.*, 2006, **97**, 266101.
3. S. N. Jamadagni, R. Godawat and S. Garde, in *Annual Review of Chemical and Biomolecular Engineering, Vol 2*, ed. J. M. Prausnitz, Annual Reviews, Palo Alto, 2011, vol. 2, pp. 147-171.
4. M. J. Stevens and G. S. Grest, *Biointerphases*, 2008, **3**, FC13-FC22.
5. P. Mark and L. Nilsson, *J. Phys. Chem. A*, 2001, **105**, 9954-9960.
6. D. Bandyopadhyay and N. Choudhury, *J. Chem. Phys.*, 2012, **136**, 224505-224510.
7. A. Luzar and D. Chandler, *Nature*, 1996, **379**, 55-57.
8. S. Balasubramanian, S. Pal and B. Bagchi, *Phys. Rev. Lett.*, 2002, **89**, 115505.
9. D. Frenkel and B. Smit, *Understanding Molecular Simulations: From Algorithms to Applications*, Academic Press, 2001.
10. R. Lavery, M. Moakher, J. H. Maddocks, D. Petkeviciute and K. Zakrzewska, *Nucleic Acids Res.*, 2009, **37**, 5917-5929.
11. Z. M. Raspopovic, S. Sakadzic, S. A. Bzenic and Z. L. Petrovic, *IEEE Transactions on Plasma Science*, 1999, **27**, 1241-1248.
12. M. F. Hagan, A. R. Dinner, D. Chandler and A. K. Chakraborty, *Proc. Natl. Acad. Sci. U. S. A.*, 2003, **100**, 13922-13927.
13. J. C. Phillips, R. Braun, W. Wang, J. Gumbart, E. Tajkhorshid, E. Villa, C. Chipot, R. D. Skeel, L. Kale and K. Schulten, *J. Comput. Chem.*, 2005, **26**, 1781-1802.
14. J. H. Monserud and D. K. Schwartz, *Biomacromolecules*, 2012, **13**, 4002-4011.